

Exploring Biomagnetism for Inclusive Vital Sign Monitoring: Modeling and Implementation

Xiuzhen Guo¹, Long Tan¹, Tao Chen², Chaojie Gu¹, Yuanchao Shu^{1,*}, Shibo He¹, Yuan He³, Jiming Chen¹, Longfei Shangguan²

¹College of Control Science and Engineering, Zhejiang University

²Department of Computer Science, University of Pittsburgh

³School of Software and BNRIst, Tsinghua University

{guoxz,gucj,ycshu,s18he,cjm}@zju.edu.cn,tanlongwork@gmail.com
{tac194,longfei}@pitt.edu,heyuan@tsinghua.edu.cn

ABSTRACT

This paper presents the design, implementation, and evaluation of MagWear, a novel biomagnetism-based system that can accurately and inclusively monitor the heart rate and respiration rate of mobile users with diverse skin tones. MagWear's contributions are twofold. Firstly, we build a mathematical model that characterizes the magnetic coupling effect of blood flow under the influence of an external magnetic field. This model uncovers the variations in accuracy when monitoring vital signs among individuals. Secondly, leveraging insights derived from this mathematical model, we present a software-hardware co-design that effectively handles the impact of human diversity on the performance of vital sign monitoring, pushing this generic solution one big step closer to real adoptions. We have implemented a prototype of MagWear on a two-layer PCB board and followed IRB protocols to conduct system evaluations. Our extensive experiments involving 30 volunteers demonstrate that MagWear achieves high monitoring accuracy with a mean percentage error (MPE) of 1.55% for heart rate and 1.79% for respiration rate. The head-to-head comparison with Apple Watch 8 further demonstrates MagWear's consistently high performance in different user conditions.

*Corresponding author; e-mail: ycshu@zju.edu.cn.

Permission to make digital or hard copies of all or part of this work for personal or classroom use is granted without fee provided that copies are not made or distributed for profit or commercial advantage and that copies bear this notice and the full citation on the first page. Copyrights for components of this work owned by others than the author(s) must be honored. Abstracting with credit is permitted. To copy otherwise, or republish, to post on servers or to redistribute to lists, requires prior specific permission and/or a fee. Request permissions from permissions@acm.org.

ACM MobiCom '24, September 30–October 4, 2024, Washington D.C., DC, USA

© 2024 Copyright held by the owner/author(s). Publication rights licensed to ACM.

ACM ISBN 979-8-4007-0489-5/24/09...\$15.00

<https://doi.org/10.1145/3636534.3649349>

CCS CONCEPTS

- Human-centered computing → Ubiquitous and mobile computing; Human computer interaction (HCI);
- Hardware → Emerging interfaces.

KEYWORDS

Wearable Health, Mobile Computing, Magnetic Sensing

ACM Reference Format:

Xiuzhen Guo, Long Tan, Tao Chen, Chaojie Gu, Yuanchao Shu, Shibo He, Yuan He, Jiming Chen, Longfei Shangguan. 2024. Exploring Biomagnetism for Inclusive Vital Sign Monitoring: Modeling and Implementation. In *International Conference On Mobile Computing And Networking (ACM MobiCom '24)*, September 30–October 4, 2024, Washington D.C., DC, USA. ACM, New York, NY, USA, 15 pages. <https://doi.org/10.1145/3636534.3649349>

1 INTRODUCTION

Vital sign monitoring, such as tracking the heart rate (HR) and respiration rate (RR), has become a popular functionality on smart wearables. By continuously monitoring the vital signs of the wearer, these wearable devices enable a broad spectrum of healthcare applications, including sleep monitoring, fitness tracking, and health issue alerting.

Nowadays, smartwatches [1, 3, 7] have emerged as the primary choice for continuous vital sign monitoring among various types of wearables. These smartwatches adopt Photoplethysmography (PPG) sensor that emits an LED beam onto the skin. The LED signal is mirrored back based on the blood volume circulating through the wrist's veins. The PPG waveform contains the pattern of the blood volume variations occurring between the systolic and diastolic phases of the cardiac cycle. The frequency of the PPG signal reflects the heart rate (HR) and respiration rate (RR). We can further leverage the filter to separate these two vital signs.

Despite their convenience, existing PPG-based smartwatches still face several crucial challenges that limit their ability to accurately monitor vital signs across diverse populations.

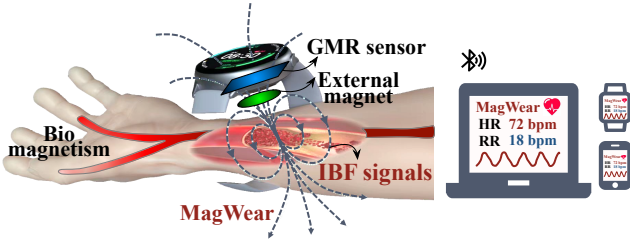


Figure 1: An illustration of MagWear. A built-in tiny magnet pushes the blood flow to generate induced biomagnetic field (IBF) signals. MagWear then leverages a GMR sensor to detect subtle changes in IBF signals to derive the heart rate and respiration rate.

- Firstly, PPG sensors are shown to be less accurate in people with dark skin [18]. This discrepancy arises due to the elevated melanin levels in darker skin, causing absorption of the laser light and consequently reducing the signal-to-noise ratio of the measurements.
- Secondly, PPG sensors often need to be worn snugly against the skin to ensure accurate readings. This can lead to discomfort, skin irritation, or even pressure-related discomfort when used for extended periods [27].
- Thirdly, the PPG sensor's accuracy can be affected by temperature variations and moisture levels of the skin, potentially leading to fluctuations in readings [31].

To overcome these issues, prior works have put forth the idea of harnessing *biomagnetism* as an alternative approach for monitoring human vital signs [25, 37]. This approach is based on a physiological process where the blood circulation within the body during each heartbeat gives rise to the movement of charged particles (ions). These ions, in turn, induce a biomagnetic field, the strength of which corresponds to the fluctuations occurring with each individual heartbeat.

Some recent investigations [25, 33] have demonstrated the potential of such an approach. However, these studies face two major challenges: *i) Usability*: Many prior studies utilize fixed deployments for both users and measuring devices. This choice stems from the exceedingly weak induced biomagnetic field, necessitating meticulous tuning of sensing parameters to ensure the capture of adequate vital information across different users. The fixed deployment serves to mitigate uncertainties introduced by factors like the distance between the user and the device. Unfortunately, this method restricts its applicability primarily to lab environments and degrades the user experience. *ii) Reliability*: Measurements from prior studies show considerable inconsistencies. The correlation between system performance and individual-specific factors like wrist size, fat thickness, and blood vessel dimensions is still not fully understood. Consequently, systems may yield unreliable results when assessing a black-box modeling signal

without a pragmatic methodology. In light of these challenges, substantial work remains before a wearable prototype can be developed for practical daily *in-situ* monitoring.

In this paper, we revisit biomagnetism and present the design, implementation, and evaluation of MagWear, the first wearable form factor design for inclusive and reliable vital sign monitoring. Figure 1 shows an illustration of MagWear, where a built-in tiny magnet pushes the blood flow to generate induced biomagnetic field (IBF) signals. MagWear then leverages a GMR sensor to detect subtle changes in IBF signals to derive the heart rate and respiration rate. To deal with the human diversity, MagWear adaptively optimizes the external excitation magnetic field to improve the SNR of IBF signals receptions, without human intervention.

The design of MagWear faces three practical challenges. **Absence of IBF signals modeling:** To date, the theoretical and practical limits of biomagnetism for human vital sign monitoring are still largely unknown. More precisely, while previous research has demonstrated the possibility of capturing slight variations in the IBF signals through giant magnetoresistance (GMR) sensors, the reasons behind the varying precision of measurements among different individuals continue to elude us. The factors causing a GMR sensor configuration to succeed in one person while proving ineffective in another remain unclear. To this end, we thoroughly analyze the generation process of IBF signals and subsequently construct a comprehensive mathematical model that serves as a theoretical foundation guiding the design of MagWear.

Addressing user-dependent IBF signals variations: Once a comprehensive understanding is gained regarding the reasons underlying the variability of measurement accuracy among different individuals, the subsequent challenge is addressing this diversity inherent to humans. A fixed GMR sensor configuration inevitably leads to a deterioration in vital sign monitoring accuracy. In order to mitigate the influence introduced by individual distinctions, we propose an online adaptive algorithm that takes the IBF signal as the feedback and automatically adjusts the sensor configurations to improve the measurement accuracy, without explicit human intervention.

Wearable integration and prototyping: As a wearable, MagWear should balance an intricate interplay of detection accuracy, power consumption, and costs. We tackle this challenge by carefully designing both the hardware layout and signal processing pipeline. Our design offloads most of the signal processing to the analog domain, striking a balance between cost and power consumption. The hardware design, on the other hand, takes into account the impact of the magnet's position on measurement accuracy to optimize the overall layout. We expect the form factor of the current prototype can be largely reduced when implemented on a flexible PCB.

We conduct extensive experiments to evaluate the performance of MagWear in various settings. The evaluation involves 30 volunteers of diverse ages and skin tones. The field studies show that MagWear achieves consistently high performance with a mean percentage error (MPE) of 1.55% for heart rate and 1.79% for respiration rate. The head-to-head comparison of HR monitoring with the commodity Apple Watch 8 shows that MagWear respectively brings reductions in estimation error, particularly in scenarios involving diverse skin tones (up to 3.8×), body hair (up to 2.6×), tattoos (up to 2.1×), and clothing (up to 6.7×).

- The contributions of this paper are summarized as follows.
- We build the first mathematical model that characterizes the magnetic coupling effect of blood flow under the influence of an external magnetic field. This model clarifies the variations in measurement accuracy observed among individuals and provides valuable guidance to improve the robustness of MagWear.
 - We propose a power-efficiency hardware-software solution that can effectively handle the human diversity on biomagnetism-based vital sign monitoring performance. The proposed solution pushes this inclusive vital sign monitoring solution one big step closer to real adoptions.
 - We implement MagWear on a one-layer PCB board and follow the IRB protocol to conduct an extensive experiment involving 30 volunteers. The results confirm the superiority and inclusiveness of our proposed solution in both heart rate monitoring and respiration rate monitoring when compared to the Apple Watch 8 baseline.

2 PRELIMINARY

MagWear explores biomagnetism, particularly the induced biomagnetic field (IBF) signals for human vital sign monitoring. In this section, we first present an overview of IBF signals (§2.1). We then summarize the key difficulties in implementing IBF-based vital sign monitoring by conducting thorough benchmarks (§2.2).

2.1 Induced Biomagnetic Field Signals Primer

As an integral component of the human cardiovascular system, arteries serve as the conduits through which oxygen-rich blood is transported from the heart to every cell in the body. In arteries, there exists a large number of hemoglobin ($C_{3032}H_{4816}O_{812}N_{780}S_8Fe_4$), which is a protein found in red blood cells (RBCs) and plays a pivotal role in oxygen transport. This functionality stems from its ability to bind oxygen to its iron component in the Fe^{2+} state. Consequently, when subjected to an external magnetic field, the iron within hemoglobin in RBCs becomes magnetically attracted, resulting in an **induced biomagnetic field (IBF)** signals as elucidated by the principles of biomagnetism [26]. The variation of

IBF signals reflects cardiovascular activities and thus can be leveraged to monitor human vital signs. It is noteworthy that the cardiovascular system operates seamlessly irrespective of whether an individual is in motion or at rest. For instance, the heart continuously contracts and relaxes, while the lungs facilitate inhalation and exhalation. These intrinsic physiological processes influence the IBF continuously. Hence, IBF signals existing within arteries contain informative data about these vital signs.

Measuring IBF Signals with GMR Sensor. Although the variation of the induced biomagnetic field signal contains a wealth of vital sign information, the strength of this signal is extremely low, making it challenging to be detected. As such, prior works leverage the **giant magnetoresistance (GMR)** unit to detect the IBF signals due to its compact form factor, low cost, and high sensitivity. GMR refers to the phenomenon in which the electrical resistivity of a magnetic material changes greatly when there is an external magnetic field nearby. There are two types of GMR units: parallel GMR and anti-parallel GMR, which means that the resistance is positively or negatively correlated with the strength of the external magnetic field. A commodity GMR sensor consists of two parallel GMR units and two anti-parallel GMR units, which form a full Wheatstone bridge [16] to measure the subtle changes in the magnetic field. The GMR sensor exhibits a null output in the absence of an external magnet. Hence it offers an intrinsic compensation for thermal drift.

2.2 Understanding IBF-based Vital Sign Monitoring Through Benchmark Studies

Despite the existing research that explores the potential of utilizing IBF signals for human vital sign monitoring, numerous practical challenges still impede the practical implementation of this approach. In this section, we follow prior works [17, 21, 25, 33, 37] to develop a GMR-based IBF measurement testbed, and conduct a comprehensive benchmark study based on 30 volunteers. The goal is to understand the efficacy and limitations of this approach.

Experiment Setups. We use a 30 mT NdFeB disc permanent magnet with a diameter of 10 mm as the external magnet, to activate the blood flow and induce the IBF signals. Then we select a general-purpose NVE AA004 [8] GMR sensor to capture the IBF signals. The temperature compensation is achieved by the internal Wheatstone design of the GMR sensor. We place the permanent magnet on the radial artery of the wrist, and the GMR sensor is placed horizontally on top of the external magnet with a distance of 10 mm. For the ground truth, volunteers wear an FDA-approved Fingertip Pulse Oximeter [6] on the index finger.

Signal Processing. Considering that the heartbeat rate of humans is usually between 60 and 100 bpm [44], we first pass

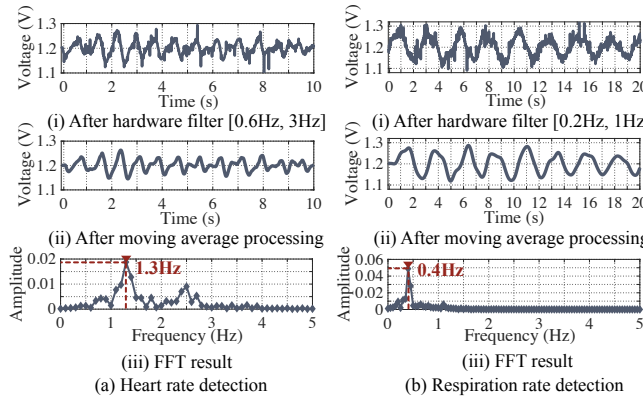


Figure 2: Feasibility study result. (a) heart rate. (b) respiration rate detection.

the signal output from the GMR sensor through a band-pass filter of [0.6 Hz, 3 Hz] to remove the DC component and the high-frequency noise. Figure 2(a-i) shows the measured IBF signals from one of the 30 experiment participants. After that, a moving average processing is applied to remove circuit noise and signal burrs. As shown in Figure 2(a-ii), the filtered IBF signals present clearly periodic characteristics. We then leverage Fast Fourier Transform (FFT) to identify the periodicity which corresponds to the heartbeat rate (HR). As shown in Figure 2(a-iii), the measured heartbeat rate is about 1.3 Hz. The respiratory rate is obtained in a similar way. The output signals from the GMR sensor first pass through a band-pass filter of [0.2 Hz, 1 Hz], since adults breathe 12 to 20 times per minute. Then we adopt FFT to identify the respiratory rate. As shown in Figure 2(b), the measured respiratory rate is about 0.4 Hz.

We have two key observations drawn from the experimental results shown in Figure 3.

- **Observation I: The vital sign monitoring accuracy varies significantly with different users.** Figure 3(a) presents the histogram of the errors of heart rate (HR) across all volunteers. The HR detection accuracy exhibits substantial variation among the 30 participants: 58% displayed commendable HR detection accuracy with errors between 0–5%; 29% had a marginally larger detection error, specifically in the 5% –10% range; and 13% showcased an even more pronounced error rate of 10% –16%. Based on the ANSI specified error criterion for cardiac monitors and HR meters [2], an error rate of 10% (or 5 bpm) is deemed significant, compromising the true reflection of a user’s cardiac health.

- **Observation II: The placement of GMR sensor greatly impacts the vital sign monitoring accuracy.** As shown in Figure 3(b), the measured IBF signals exhibit different HR accuracy when the GMR sensor is placed in four different ways (position & orientation). Specifically, when the GMR

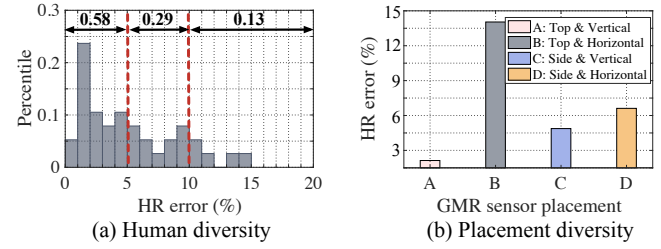


Figure 3: Benchmark results demonstrate the impact of (a) human diversity and (b) placement diversity of GMR sensor on IBF signals detection.

sensor is positioned horizontally above the external magnet, the heart rate detection yields a minimal error of 1.48%. Conversely, placing the GMR sensor vertically atop the external magnet results in a substantial increase in heart rate detection error, reaching up to 13.8%. Similarly, the two alternative positions were tested, revealing a reduction in detection error to approximately 4.7% and 6.5%, respectively.

Summary. These above observations will contribute to the vital sign monitoring based on the IBF signal to practical use. In order to address the aforementioned challenges, the priority is to understand the reasons. We conducted an extensive literature review, yet we were unable to find any explanations. This motivates us to build a mathematical model to figure out the factors responsible for the variability in performance. Hence, we first model IBF signal generation (§3) to understand how human diversity affects vital sign monitoring performance. Under the guidance of this model, we then propose an effective hardware-software solution to mitigate the impact of human diversity (§4). Finally, we optimize the placement of GMR sensors in our wearable design to improve the vital sign monitoring performance (§5).

3 THEORETICAL ANALYSIS OF IBF

Starting from the Hall effect, we build a mathematical model to understand IBF signal generation (§3.1). This model not only explains the disparities observed in vital sign monitoring effectiveness across various users but also provides valuable insights to improve the robustness of MagWear (§3.2).

3.1 Modeling IBF Signal Generation

We model the relationship between the external magnetic field (EMF) signals and the induced biomagnetic field (IBF) signals, and then quantitatively analyze various factors that affect the IBF signals.

Inspired by the Hall effect [9], we added an external magnet over the blood vessel to generate the IBF signals. As shown in Figure 4(b), according to the left-hand rule, the charged particle (like Fe^{2+}) will feel Lorentz force F and it can be

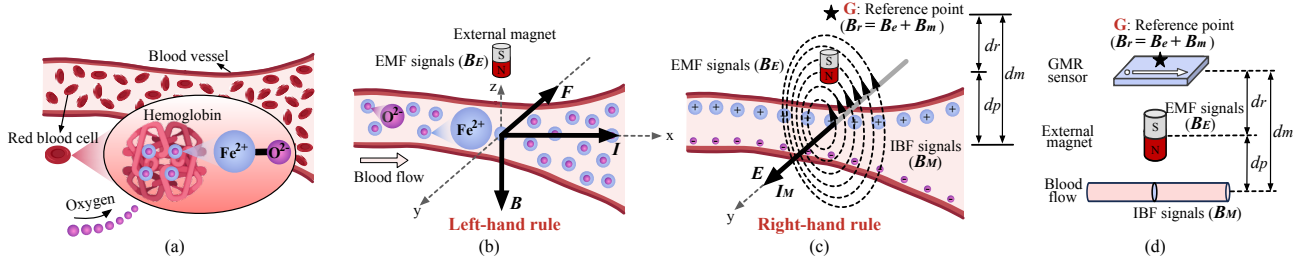


Figure 4: Detection theory of MagWear. (a) Structure of the arterial vessel. (b) The positive ions in the arterial vessel are subject to Lorentz forces when the external magnet is applied. (c) Under the influence of Lorentz force, positive and negative ions move towards both sides of the blood vessel, and generate induced current and induced biomagnetic field (IBF) signals. The IBF signals will further affect the magnetic flux at the reference point. (d) Model abstraction.

calculated by:

$$\mathbf{F} = q \cdot \mathbf{v} \times \mathbf{B} \quad (1)$$

where q is the charge of the particle, v is the speed of the particle, and B is the magnetic field strength felt by the particle.

Under the influence of the Lorentz force, charged particles continuously move in the direction of the Lorentz force and generate an electric field. As shown in Figure 4(c), when the Lorentz force and the electric field force reach equilibrium, we can obtain the following relationship:

$$\mathbf{q} \cdot \mathbf{v} \times \mathbf{B} = \mathbf{E} \cdot \mathbf{q} \quad (2)$$

where E is the electromotive force generated by the positive and negative particles, and we have $E = v \times B$. The induced current I_M generated under this electric field is:

$$I_M = \frac{\mathbf{E}}{R_0} = \frac{\mathbf{v} \times \mathbf{B}}{R_0} \quad (3)$$

where R_0 is the resistance of blood flow.

According to Ampère's right-hand rule, the induced current generates the IBF signals, and the strength of the IBF signals B_M is:

$$B_M = \frac{\mu_0 I_M \times \mathbf{e}_r}{2\pi r} = \frac{\mu_0 v \times B \times \mathbf{e}_r}{2\pi r R_0} \quad (4)$$

where μ_0 is the magnetic permeability, \mathbf{e}_r is the vertical component of the current vector, and r represents the distance from the induced current.

Detecting the IBF signals. In practice, we detect the variation in IBF signals by measuring the magnetic field at a point above the blood vessel, *e.g.*, the reference point "G" shown in Figure 4(c) and Figure 4(d). Now let's assume the strength of the external magnet is B_E , the distance from the external magnet to the reference point, from the external magnet to the blood vessel, and from the blood vessel to the reference point is d_r , d_p , and $d_m = (d_r + d_p)$, respectively. Then the EMF signals at the reference point "G" can be written as $B_e = h \frac{B_E}{d_r^3}$. Likewise, the IBF signals generated by the blood flow at the reference point "G" can be represented as $B_m = \frac{\mu_0 v \times B \times \mathbf{e}_r}{2\pi(d_r + d_p)R_0} =$

$\frac{\mu_0 v \times B_E \times \mathbf{e}_r}{2\pi(d_r + d_p)d_p^3 R_0}$. Hence the overall magnetic field sensed by the GMR sensor at point "G" is:

$$B_r = B_e + B_m = \underbrace{h \frac{B_E}{d_r^3}}_{EMF \text{ signals}} + \underbrace{\frac{\mu_0 v \times B_E \times \mathbf{e}_r}{2\pi(d_r + d_p)d_p^3 R_0}}_{IBF \text{ signals}} \quad (5)$$

From the above equation, we have two observations.

- Firstly, the output of the GMR sensor reflects the variation of IBF signals since the EMF signals are constant under a fixed GMR sensor setup. This equation demonstrates the theoretical potential of utilizing IBF signal measurements for monitoring human vital signs.

- Secondly, this equation offers insights into the parametric factors that influence IBF signals, including the magnetic permeability μ_0 , speed of particles v , the distance from the external magnet to the blood vessel d_p , and the resistance of the blood flow R_0 , all of which are affected by human wrist size, fat thickness, and blood vessel dimensions. Accordingly, when applying the same measurement setup to different users, we are expected to get IBF signals in different SNRs. This essentially explains the variations we observed in the heart rate monitoring performance across different users (Figure 3).

3.2 Takeaways from the IBF Modeling

To ensure that MagWear can detect the heart rate accurately across different users, it's crucial to improve the SNR of IBF signals measured at each user. According to Equation 5, there are two potential solutions to improve the SNR of each individual's IBF signals.

- The first solution is to minimize the separation between the external magnet and the reference point as well as the blood flow (*i.e.*, d_r and d_p) by moving the external magnet around. However, from the usability perspective, it is usually inconvenient to require the user to manually adjust the position of this magnet and the wrist while monitoring.

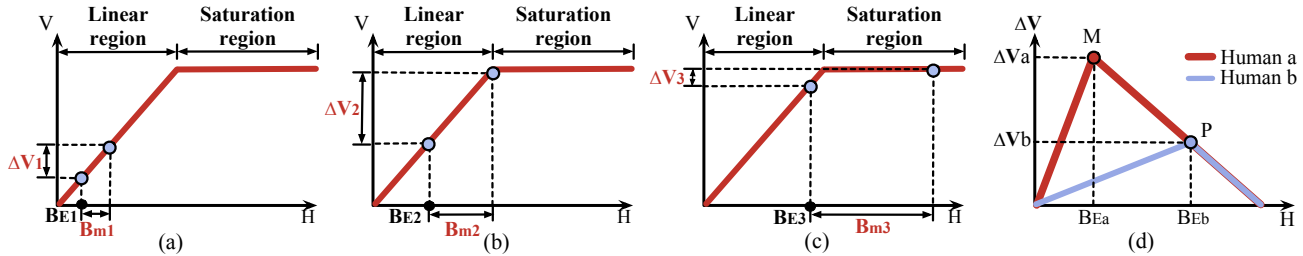


Figure 5: (a–c) Output signal strength of the GMR sensor when applying different external magnetic fields; (d) The relationship between the GMR sensor's output amplitude and the external magnet strength.

• Another solution is to increase the intensity of the external magnetic field B_E by using a more potent external magnet. While this approach eliminates the need for manual magnet positioning, it encounters two technical obstacles. First, how to make changes to the intensity of the external magnetic field freely, without explicit human intervention? Adding multiple magnets with varying strengths would unavoidably augment the dimensions and weight of MagWear. Second, how to find the best external magnetic field configuration for each individual? Blindly using a stronger magnet does not necessarily guarantee a higher heart rate monitoring accuracy as the magnetic field intensity may saturate the GMR sensor reading, resulting in an inferior monitoring accuracy.

Figure 5 explains this issue. Initially, when a low-intensity external magnetic field is applied (Figure 5(a)), the resultant induced biomagnetic field (IBF) signal would exhibit a low strength (as per Equation 5). Consequently, the variation B_{m1} stemming from the heartbeat would be subtle, yielding a relatively minor GMR sensor reading ΔV_1 . This scenario presents a significant hurdle to achieving accurate heart rate monitoring. As we gradually increase the intensity of the external magnetic field, the IBF signal strength also grows, which results in a more pronounced GMR sensor reading ΔV_2 , as shown in Figure 5(b). In this case, we are expected to get a more accurate heart rate measurement.

As the external magnetic field intensity is elevated even more (as depicted in Figure 5(c)), the potency of the induced IBF signal would exceed the GMR sensor's effective detection range, entering a saturation region where alterations in the GMR sensor reading cease despite escalating IBF signal strength. Consequently, the amplified fluctuation in the IBF signal (B_{m3}) caused by the heartbeat merely corresponds to a minimal change in GMR readings (ΔV_3), ultimately leading to suboptimal accuracy in monitoring heart rate.

To improve the heart rate monitoring accuracy, we should optimize the external magnetic field to ensure that the highest IBF signal strength resides within the boundary between the GMR sensor's effective detection range and its saturation region. As the curve shown in Figure 5 changes with different

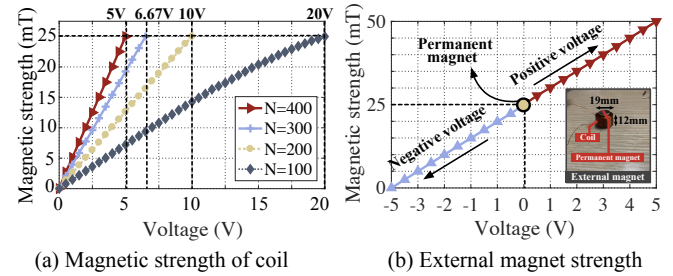


Figure 6: (a) The intensity of the electromagnet grows with the bias voltage and the number of turns the coil has. (b) External magnet strength.

users, it's crucial to put forward an online algorithm that can automatically adapt the IBF signals for different users.

4 AUTOMATIC IBF SIGNAL TUNING

In this section, we present a software-hardware co-design approach that can automatically tune the IBF signal for each individual. We first describe the programmable external magnetic field design (§4.1) that allows us to freely change the intensity of the external magnetic field. We then present our online IBF signal tuning algorithm (§4.2).

4.1 Programmable External Magnetic Field

We build a programmable external magnetic field (EMF) module based on the electromagnetic induction phenomenon – when an electric current traverses a coil, it generates an encompassing magnetic field [4]. The potency of this magnetic field is modulated by variations in the electric current. As a result, we can manipulate the electric current to create the intended external magnetic field.

In our system, we realize this programmable EMF module using a copper coil with a diameter of 19 mm and a height of 12 mm. Note that the electromagnet consumes extra energy, thus, to prolong the battery time of MagWear, we further take into account the following factors when putting forward this programmable EMF module.

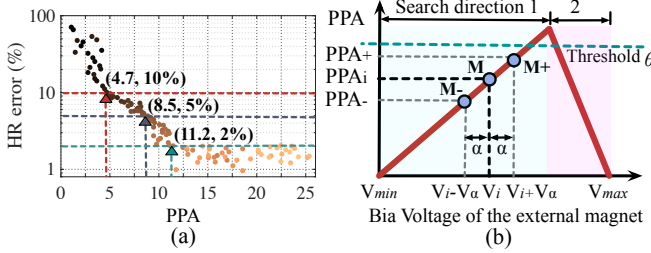


Figure 7: (a) A metric of PPA to describe the signal quality; **(b)** The relationship between PPA and the bias voltage of the external magnet.

- Firstly, the programmable EMF module is constructed by overlaying an electromagnet on a permanent magnet. The external magnetic field is the superposition of the permanent magnet and the electromagnet. The permanent magnet provides a basic magnetic bias and the electromagnet is used to adjust the external magnetic strength. This hybrid architecture essentially reduces the size, weight, and power consumption of MagWear.

- Secondly, the intensity of the programmable electromagnetic field is proportional to the number of coil turns and the magnitude of the bias voltage, as shown in Figure 6(a). Given the same magnetic strength requirement, the more turns the coil has, the lower the required bias voltage. Note that, in our design we choose a coil with 400 turns to minimize the required bias voltage, thereby reducing the power consumption.

- Thirdly, altering the direction of current flow within the electromagnetic setup can result in a change in the electromagnetic field's direction. This allows us to expand the range of the intensity of this programmable EMF module. For instance, an external magnetic field of [0, 50 mT] can be built by overlaying an electromagnet of [-25 mT, 25 mT] on a permanent magnet of 25 mT, as shown in Figure 6(b).

4.2 Online IBF Signal Tuning Algorithm

The strength of the IBF signal is proportional to the intensity of the external magnetic field, making it possible to adjust the IBF signal by modifying the bias voltage applied to the programmable EMF module. However, as discussed in §3.2, the IBF signal strength is crucial for accurate vital sign monitoring and thus should not be tuned arbitrarily. On one hand, if the IBF signal is tuned to be excessively small, its fluctuations resulting from the heartbeat might become too small to be detected by the GMR sensor. Conversely, if the IBF signal is adjusted to an excessive strength (for instance, entering the saturation region), the signal variations become undetectable by the GMR sensor as well (Figure 5(c)).

In MagWear, we introduce a feedback-loop algorithm designed for tuning IBF signals. This online algorithm employs

Algorithm 1: Online adaptive tuning algorithm

```

input :  $V_{min}, V_{max}$ ; // voltage range
 $V_\alpha$ ; // voltage tuning step length
 $N$ ; // maximum search attempts
 $\theta \leftarrow \{4.7, 8.5, 11.2\}$ ; // PPA thresholds
 $\theta_t \leftarrow 4.7$ ;  $i \leftarrow 0$ ;
output : Feasible bias voltage  $V_{out}$ ;
1 while  $\theta_t$  is in  $\theta$  and  $i \leq N$  do // initialization
2    $V_i \leftarrow \frac{V_{min}+V_{max}}{2}$ ;
3    $PPA_i \leftarrow \text{CompPPA}(V_i)$ ;
4   if  $PPA_i \leq \theta_t$  then // decide search direction
5      $PPA_+ \leftarrow \text{CompPPA}(V_i + V_\alpha)$ ;
6      $PPA_- \leftarrow \text{CompPPA}(V_i - V_\alpha)$ ;
7     if  $PPA_+ \geq PPA_-$  then // binary search
8        $V_{min} \leftarrow V_i$ ;
9        $V_i \leftarrow \frac{V_{min}+V_{max}}{2}$ ;
10      return  $V_i$ ;
11    else
12       $V_{max} \leftarrow V_i$ ;
13       $V_i \leftarrow \frac{V_{min}+V_{max}}{2}$ ;
14      return  $V_i$ ;
15  else
16    Update  $\theta_t$ ; // update a tighter threshold
17   $i++$ ;

```

the past IBF signal reading (provided by the GMR sensor) as a reference to fine-tune the bias voltage of the electromagnet, aiming to maximize the SNR of the IBF reading.

We first characterize the SNR of the IBF signal readings. In particular, we choose **Peak-Peak to Average ratio** (PPA) metric to characterize the quality of the received IBF signals. The PPA is defined as the peak-to-peak intensity within [0.6 Hz, 3 Hz] frequency band¹ over the average signal intensity within this band. To validate the effectiveness of our signal quality metric, we depict both the PPA and the heartbeat detection error for a group of 30 volunteers in Figure 7(a). Evidently, the error rate reduces to its minimum and becomes stable when the PPA exceeds 2%.

Algorithm 1 outlines the IBF signal tuning process. Our algorithm searches for the optimal bias voltage within a voltage range. Each time we compare the current PPA value with that corresponding to the intermediate voltage, then we reduce the search range by half until we find the optimal bias voltage. This process is similar to the binary search. Specifically, the function *CompPPA()* is called to obtain the PPA of the received IBF signal in the current bias voltage input settings. Let the range $[V_{min}, V_{max}]$ denote the voltage limits of the electromagnet, which govern the boundaries for the magnetic strength value of B_E . The initial bias voltage of the electromagnet V_i is set to $(V_{min} + V_{max})/2$.

To expedite the search process, we leverage the monotonic properties of the PPA metric and adjust the acceptable HR

¹ where heartbeat signal stays.

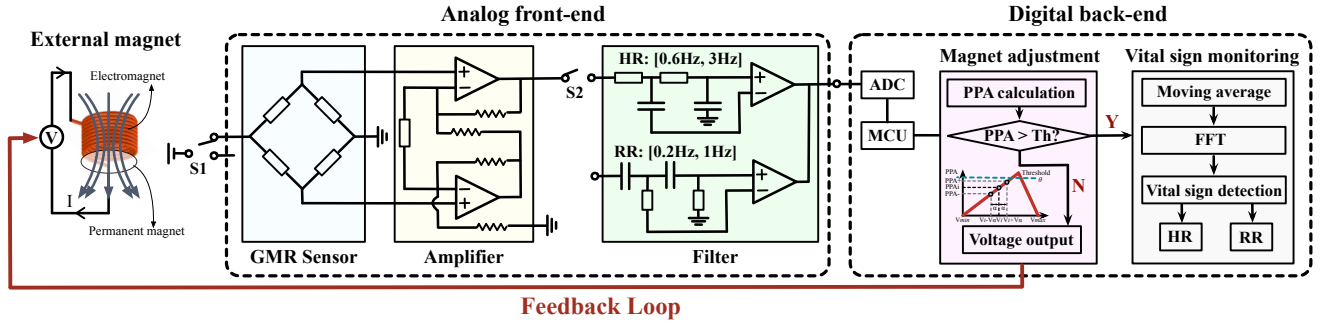


Figure 8: The schematic of MagWear.

threshold in response to user variations. Taking Figure 7(b) as a reference, if PPA_i of the received IBF signal is less than a PPA threshold θ , the algorithm updates the bias voltage to $(V_i + V_\alpha)$ and $(V_i - V_\alpha)$ and gets two PPA readings, namely PPA_+ and PPA_- , based on these two bias voltage settings. V_α is the voltage tuning step length and it can be dynamic. The step size decreases as the PPA value approaches the maximum value. These two PPA values essentially discern the slope's direction of the PPA curve (*i.e.*, point M_+ and M_-). After identifying the direction (by comparing PPA_+ with PPA_-), the algorithm runs a binary search (lines 4–14) to narrow down the search space, expediting the searching. The binary search is lightweight and can run on a microcontroller efficiently. The initial PPA threshold θ is empirically set to 4.7. It grows whenever the searched result meets the HR error limits.

Tradeoff between the SNR and battery life. The external magnetic field intensity directly impacts the SNR of the IBF signal, consequently influencing the detection accuracy of MagWear. Our online tuning algorithm can automatically adjust the strength of the external magnet, thus adapting the IBF signals for different users. While the following algorithm optimizes SNR performance, it also incurs a consumption of battery energy due to the search process. Our empirical study demonstrates that within 100 search attempts (around 12 seconds), the algorithm is capable of identifying an appropriate bias voltage configuration that results in heart rate errors below 5% for over 99% of the subjects.

5 IMPLEMENTATION

5.1 MagWear Prototype

We prototype MagWear on a two-layer printed circuit board (PCB) using COTS analog components and an ultra-low power ESP32 MCU [14]. Figure 8 and Figure 9 show the hardware schematic and the hardware prototype. MagWear consists of three parts: (1) external magnet, (2) analog front-end, and (3) digital back-end. The prototype costs approximately \$15.3 USD.

- **External magnet.** After a series of initial experiments, we empirically select the external magnet of [0, 50 mT] to induce the IBF signals. This external magnet is built by overlaying an electromagnet of [-25 mT, 25 mT], a pure copper coil with 400 turns, on a permanent magnet of 25 mT. The size of the external magnet is 19 mm × 12 mm.

- **Analog front-end.** We adopt NVE AA004 [8] GMR sensor to detect IBF signals. The output of the GMR sensor is connected to a low-power amplifier composed of INA126 [11] with an amplification gain of 800. With this setting, the variation of the IBF can be captured and amplified. The output signal from the amplifier is further sent to the filtering processing circuit. There are four different low-pass filters composed by OP07 [15] from Texas Instruments, and their cutoff frequencies are 0.2 Hz, 0.6 Hz, 1 Hz, and 3 Hz. By cascading these low-pass filters, two different bandpass filters [0.6 Hz, 3 Hz] and [0.2 Hz, 1 Hz] can be formed to filter out the desired heart-beat signals and respiratory signals, respectively. Then the filtered analog signals are shifted to 0-5V by a voltage converter² and are forwarded to the digital back-end. There are two switches, where " S_1 " enables MagWear to enter working mode and " S_2 " is used to select the suitable filter.

- **Digital back-end.** We adopt a 12-bit ADC with a sampling rate of 100 Hz to digitalize these analog signals and send these data to the ESP32 [14] MCU. The MCU is responsible for (a) magnet adjustment: dynamically controlling the bias voltage of the electromagnet via a driver OPA549 [10]; (b) vital sign monitoring: measuring HR and RR after signal processing.

5.2 Practical Considerations

- **Placement of the GMR Sensor.** We carefully understand the impact of GMR sensor's placement (position & orientation) on the detection result of MagWear, as elaborated in Figure 10: (1) Top & horizontal : Both the EMF signals and the IBF signals only have the horizontal component. Thus the output voltage of the GMR sensor has a good SNR and exhibits clearly distinguishable signal features. (2) Top &

² ADC can only sample positive voltage signals.

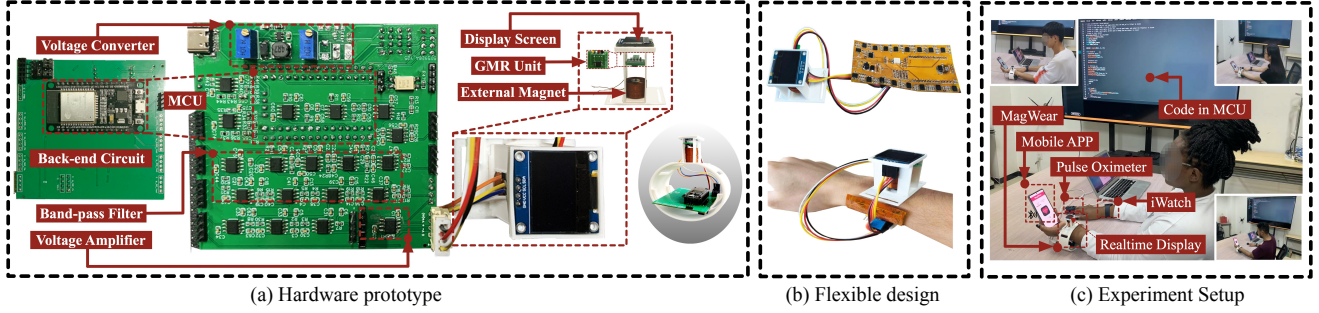


Figure 9: The prototype of MagWear and experiment setup.

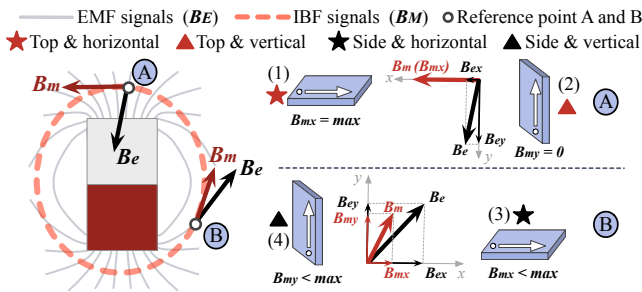


Figure 10: The placement of GMR sensor impacts the detection result of MagWear.

vertical: There is almost no signal component of IBF in the vertical direction. (3/4) Side & horizontal and side & vertical: Both the EMF signals and the IBF signals have horizontal and vertical components. However, the decomposition of IBF signals in two directions will affect the response sensitivity of the GMR sensor. The experimental result in Figure 3(b) is consistent with our above analysis. Hence, we place the GMR sensor horizontally on the top of the external magnet to maximize its detection sensitivity.

- **Device miniaturization.** MagWear has miniaturized its form factor with the following two approaches: 1) We have refined the electromagnet's profile by adopting an inside-to-outside winding pattern. Different from the traditional top-to-bottom coil winding configuration, this approach yields a significant reduction in its volume; 2) We have adopted a flexible PCB design, illustrated in Figure 9(b), to compact the circuitry. This design approach enables the prototype to be comfortably worn on the user's wrist. The miniaturization of MagWear could be further improved by adopting the Application Specific Integrated Circuits (ASIC) design during batch production.

- **Magnet Safety.** The Magnet Safety Guideline from ACGIH dictates that a magnetic field strength of up to 60mT is deemed safe for whole-body exposure, while the extremities can tolerate up to 600 mT [12, 22]. The most potent magnet in MagWear generates a magnetic field strength of less than 50 mT. This safety assurance is akin to that of headphones, which generate magnetic signals when converting electrical signals

into mechanical waves. It's also possible to minimize the strength of the magnetic signal increasing the gain of the amplification circuit. Certain individuals, especially those with cardiac implants, should exercise extra caution. Their safe exposure limit is much lower, capped at 0.5 mT. We strongly advise such individuals to seek counsel from their healthcare providers before using the device [13].

- **Electromagnetic interference.** While MagWear primarily detects IBF signals to monitor vital signs, other external magnetic interference may also affect the system's detection outcomes. The impact of such electromagnetic interference on MagWear is discussed in detail in Section §6.3. To mitigate the effects of these external interferences, a shield case can be integrated in MagWear.

- **Impact of MagWear on smart devices.** One may wonder if MagWear interferes with the smartphone's magnetometers as it actively emits a magnetic field. Our evaluations reveal that this interference is barely negligible with a distance exceeding 10 cm between MagWear and the smartphone. Meanwhile, the magnetic field generated by MagWear does not negatively impact communication protocols such as BLE and 4G/LTE/5G. This is comprehensible given that modern wireless charging technologies are built upon electromagnetic induction principles, and wireless communication would not be affected by such electromagnetic induction. Additionally, the magnetic field from MagWear doesn't destroy the internal circuits of smart devices, due to the inherent protective measures against electromagnetic interference present in these devices.

6 EVALUATION

6.1 Experiments Setup

Data collection. We recruit a total of 30 volunteers (20 males, 10 females) with different ages (21–57 years old), weights, and heights (BMI ranges from 15.9 to 31.8). As shown in Figure 9(c), the volunteers wear MagWear in a way they feel comfortable. The ground truth is obtained by an FDA-approved device, LEPU PO6 Fingertip Pulse Oximeter [6]. Our testing protocol involves each user undergoing 5-minute assessments repeated 10 times.

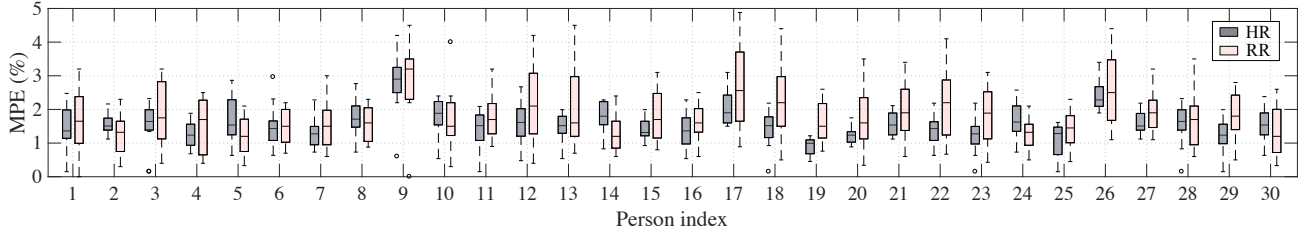


Figure 11: Overall performance

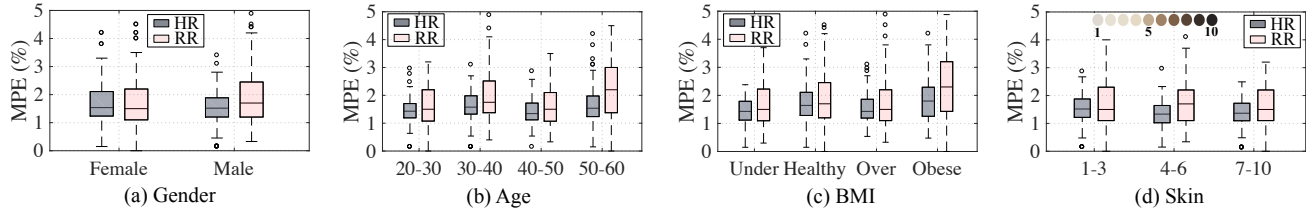


Figure 12: MagWear performance across different genders, ages, BMIs, and skin tones.

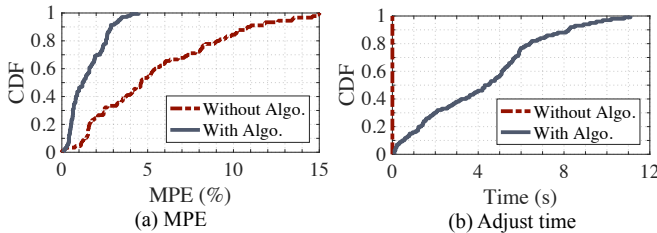


Figure 13: Performance of programmable design. (a) MPE. (b) Adjust time.

Evaluation metrics. To comprehensively evaluate MagWear’s performance, we adopt Mean Absolute Error (MAE) and Mean Percentage Error (MPE) in the evaluation. MAE characterizes the absolute error and MPE characterizes the relative error. These two metrics yield consistent evaluation results from different dimensions. The definitions of these two metrics are as follows.

- (i) *Mean Absolute Error (MAE)* is the mean absolute difference between the estimated value (denoted by V^E) and the ground truth (denoted by V^T) i.e., $MAE = \frac{1}{N} \sum_{i=1}^N |V_i^E - V_i^T|$.
- (ii) *Mean Percentage Error (MPE)* is the mean percentage difference between V^E and V^A , i.e., $MPE = \frac{1}{N} \sum_{i=1}^N \frac{|V_i^E - V_i^A|}{V_i^T}$.

6.2 Field Study

Overall performance. We first examined the HR and RR monitoring accuracy among 30 volunteers. The results are summarized in Figure 11. Overall, MagWear achieves decent performance across all 30 participants, with a mean MPE of 1.55% for HR and 1.79% for RR, respectively. We find that subjects 9, 17, and 26 have relatively higher MPE ($>2\%$) than the remaining subjects. This could likely be attributed to the fact that these individuals tend to have higher body weights. Additionally, external magnetic fields might not readily stimulate and attenuate following encounters with bodily factors.

Impact of genders. Next, we investigate the influence of gender on the accuracy of MagWear. Illustrated in Figure 12(a), our analysis reveals that MagWear remains robust across genders. Specifically, the MPE for HR is 1.67% for females and 1.51% for males. Similarly, the MPE for RR is 1.68% for females and 1.87% for males.

Impact of ages. We delve into the influence of age by categorizing our 30 participants into four groups. As depicted in Figure 12(b), we observe that the variance in MPE for HR and RR among these groups is 0.21% and 0.62%, respectively. The age group spanning 50-60 years exhibits a relatively higher MPE, particularly in terms of RR measurement. This trend can likely be attributed to the diminishing intensity of both heartbeat and respiration activity as individuals age.

Impact of BMIs. We then examine the impact of different Body Mass Index (BMI) on MagWear’s performance. We divide 30 participants into four groups, namely, underweight ($BMI \leq 18.4$), healthy ($18.5 \leq BMI \leq 24.9$), overweight ($25.0 \leq BMI \leq 29.9$), and obese ($BMI \geq 30.0$). As shown in Figure 12(c), four groups achieve HR’s MPE of 1.46%, 1.56%, 1.42%, 1.63%, and RR’s MPE of 1.58%, 1.98%, 1.53%, 2.15%. We find that the MPE of MagWear is relatively higher for obese subjects. This is expected since the blood vessels of obese subjects are deeper from the skin surface, and the IBF signal will experience more attenuation.

Impact of skin tones. Different from the PPG sensor that is sensitive to the optical path, MagWear is resilient to the skin tone, as shown in Figure 12(d). The mean MPE of HR and RR for different skin tones does not exceed 1.51% and 1.77%.

Ablation study. First, we conduct ablation experiments to evaluate the performance of our programmable design. Figure 13(a) and Figure 13(b) show the detection accuracy and

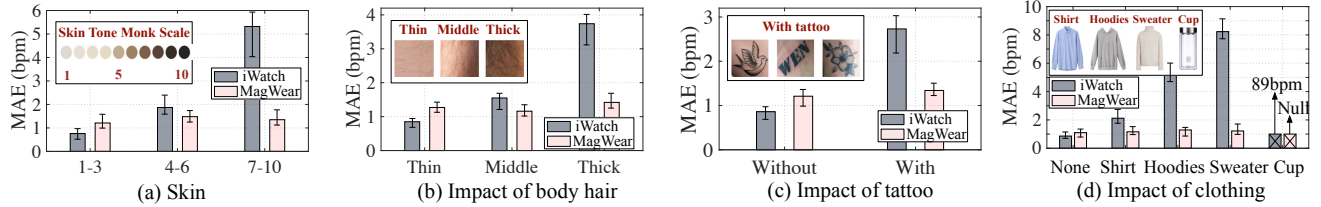


Figure 14: MagWear performance under different settings of (a) skin tone, (b) body hair, (c) tattoo, (d) clothing.

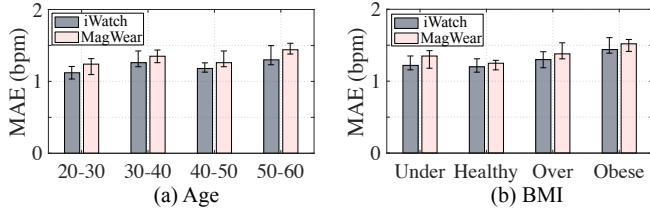


Figure 15: MagWear performance under different settings of (a) age, (b) BMI.

time delay, respectively. According to the experimental results, we find that our programmable design can significantly reduce MPE. MPE with the tuning algorithm can reduce the average MPE by $3.67\times$ from 5.46% to 1.49%. MPE is always less than 5% for all volunteers. Concurrently, the average time delay introduced by our programmable design measures 5.45 s, with the maximum delay not exceeding 12 s. This level of time delay remains well within acceptable bounds for practical applications because it is a one-time effort.

6.3 Comparison with Apple Watch

Taking the HR measurement as an example, we conduct micro-benchmarks to compare MagWear’s performance with the commercial Apple Watch. We select the most current iteration, i.e., iWatch 8 [3], and correctly wear the iWatch according to the instructions of the Apple Watch. Note that iWatch leverages a PPG sensor to perform vital monitoring. As a product-oriented wearable, iWatch requires the user to input personal data, such as birthday, height, weight, and habits, to conduct HR monitoring. Thus, iWatch can always output an estimated value, even in some corner cases. Different from iWatch, MagWear adopts a pure data-processing method that does not require any personal information of the user. Next, we evaluate MagWear’s performance under different factors, including skin color, body hair thickness, tattoo, clothing materials, age, BMIs, and long-term measurements.

Impact of skin conditions. Given classical PPG’s sensitivity to skin tone, our primary goal is to understand the inclusiveness of MagWear to the specific study population. Our IRB doesn’t mandate specific quotas for recruiting participants based on skin tones. Instead, our recruitment process is open to all skin-tone volunteers. Upon recruitment, each participant is asked to self-identify their skin tone. We recruit a total of 30 volunteers and the participant distribution is as follows: 13 out of 30 participants chose a skin tone rating of 1-3, 12

participants opted for 4-6, and 5 participants selected 7-10 on the scale. Although we haven’t covered the entire Monk scale with the balanced representation of the sample, we hold confidence that our findings will generalize to a more diverse and expansive population.

The outcomes are presented in Figure 14(a). Notably, MagWear consistently achieves low MAEs ranging from 1.21% to 1.48% across all three skin tone groups, underscoring its inclusiveness across different skin tones. In addition, a balanced representation of participants across the entire spectrum of monk-scale skin tones is a more appropriate setup. In the future, one may recruit more volunteers, leveraging a larger dataset to make the participant distribution with different skin colors more uniform, to make this technique applied better in practice.

Impact of body hair. Next, we evaluate the impact of body hair, and Figure 14(b) shows the result. As the thickness of body hair increases, the MAE of iWatch grows by $4.4\times$ from 0.85% to 3.74%, while the MAE of MagWear is relatively stable at 1.27%–1.42%. This is expected since compared to magnetic signals, optical signals are more susceptible to the occlusion of the body hair.

Impact of tattoo. Tattoos affect the propagation of optical signals. As shown in Figure 14(c), the MAE of iWatch with tattoo grows up to 2.73%, $2.04\times$ higher than that of MagWear.

Impact of clothing. We then evaluate the impact of clothing to verify the non-contact characteristic of MagWear. Volunteers wear different clothes and then wear MagWear and iWatch on their wrists. As shown in Figure 14(d), when the thickness of the clothes increases, the MAE of MagWear grows by $1.1\times$ from 1.10 bpm to 1.22 bpm, the MAE of iWatch grows by $9.56\times$ from 0.86 bpm to 8.23 bpm. Note that the magnetic flux can penetrate through the clothing, the detection result of MagWear is more reliable and sensitive than that of iWatch. In contrast, clothing obstructs the optical path between the PPG sensor and blood flow, causing the HR measurements obtained by the iWatch through clothing to effectively represent blind estimations. Remarkably, the iWatch can still yield results when placed against objects.

Impact of age. Then we examine the impact of the user’s age to verify MagWear’s robustness. 30 volunteers of different ages wear MagWear and iWatch to detect HR. The result is shown in Figure 15(a). We have the following observation.

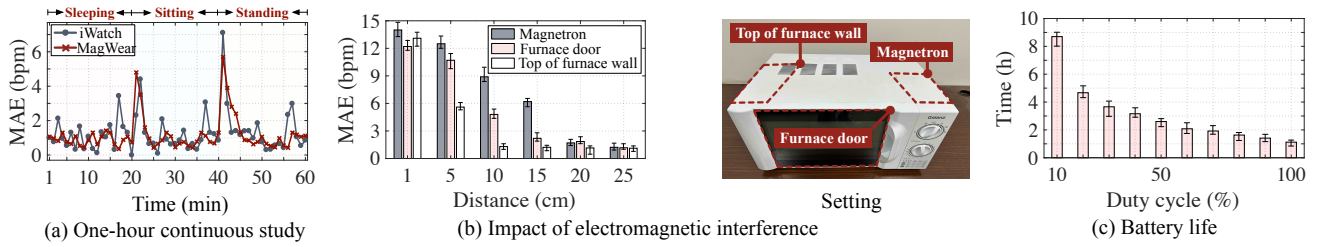


Figure 16: (a) One-hour study on a person with dark skin. (b) Impact of electromagnetic interference. (c) Battery life.

MagWear and iWatch present similar MAE errors. The MAE of MagWear and iWatch vary from 1.24 bpm to 1.44 bpm and from 1.12 bpm to 1.31 bpm, respectively. In addition, the age group spanning 50-60 years exhibits a relatively higher MAE.

Impact of BMIs. We then compare the impact of different BMIs on MagWear's and iWatch performance. We divide 30 participants into four groups, namely, underweight ($BMI \leq 18.4$), healthy ($18.5 \leq BMI \leq 24.9$), overweight ($25.0 \leq BMI \leq 29.9$), and obese ($BMI \geq 30.0$). As shown in Figure 15(b), iWatch achieves MAE of 1.22 bpm, 1.20 bpm, 1.31 bpm, 1.44 bpm for four groups, and MagWear achieves MAE of 1.35 bpm, 1.25 bpm, 1.38 bpm, 1.52 bpm. We find that the MPE of MagWear and iWatch is relatively higher for obese subjects.

One-hour continuous wearing study. We invite a participant with a darker skin tone to wear MagWear for an hour in daily activities, comprising periods of napping, sitting, and standing. The resulting data is illustrated in Figure 16(a). The average MAE of MagWear and iWatch is 1.53% and 1.548%, respectively. The MAE of MagWear is more stable than that of iWatch, which means that MagWear exhibits relatively stable characteristics in long-term measurements. Furthermore, during the transition phases between different activities, both MagWear and iWatch experience brief upticks in MAE. This can be attributed to the readjustment required as the subject transitions between distinct physiological states.

6.4 Other Issues

Impact of electromagnetic interference. To evaluate MagWear's performance under electromagnetic interference. We place the system at different distances from the different parts of a microwave oven (magnetron, furnace door, and top of furnace wall) [5]. The result is shown in Figure 16(b). Firstly, MagWear's MAE in the presence of interference is more compromised around the magnetron than around the furnace door and top of the furnace wall. The MAE values for MagWear are measured at 14.1 bpm, 12.2 bpm, and 13.1 bpm when positioned at a distance of 1 cm from the magnetron, furnace door, and top of the furnace wall, respectively. Secondly, the MAE decreases as the distance from the interference source increases. Specifically, as the separation grows to 20 cm, 15 cm, and 10 cm, the MAEs are lower than 2 bpm. This trend

Table 1: Energy consumption (active mode) and cost of each component in MagWear.

Component	GMR sensor	Voltage amplifier	Filter	ADC	MCU	External magnet	Total
Energy (mA)	1.1	1.4	2.3	145	46	243	438.8
Cost (\$)	5.6	2.7	0.4	1.9	3.5	1.2	15.3

aligns with expectations, as the magnetic field intensity of the microwave oven attenuates exponentially with distance. Thus, the influence of electromagnetic interference on MagWear remains constrained, and we can implement a shielding layer to further safeguard the system's external magnets.

Power consumption and cost. Table 1 summarizes the power consumption and cost of each component in MagWear. Under a supply voltage of 5 V, the GMR sensor, voltage amplifier, filter, ADC, and MCU consume the current of 1.1 mA, 1.4 mA, 2.3 mA, 145 mA, and 46 mA. The external electromagnet controlled by the motor driver consumes a current of 243 mA depending on the bias voltage. In total, MagWear consumes around 438.8 mA while the HR and RR measurement is running. When MagWear is in an idle state, only 0.8 mA is drawn. Thus, a 542 mAh Li-Po battery can be used to provide up to 1.24 hours of continuous measurement. We steply control the switching frequency of switch "S1" (Figure 8) to adjust the duty cycle of MagWear from 10% to 100%, and measure the battery life. As shown in Figure 16(c), the battery life drops with the increase of the duty cycle. When the duty cycle varies from 10% to 100%, the battery life drops from 8.65 h to 1.12 h. A MagWear device costs approximately US\$15.3. The cost can be reduced further through large-scale production and Application Specific Integrated Circuit (ASIC) fabrication.

7 RELATED WORK

Physiological sensing with wearables. The ever-developing Internet of Things (IoT) [19, 23, 24, 28, 29, 32, 42, 45–48, 51] brings the prosperity of wearable sensing. Existing wearable devices [23, 24, 47] predominantly employ PPG [20], ECG [35], and IMU [36] sensors for vital sign monitoring. For instance, devices like Apple Watch, Garmin Watch, and Fitbit leverage PPG sensors to facilitate heartbeat and respiratory detection. Although the PPG has been well explored and validated for everyday usage, it is not without flaws. Notably, PPG sensors have shown sensitivity towards various

skin tones, producing biased readings, especially for darker skins [18]. Departing from optical methods, ECG sensors are popular in clinical settings for their robust performance across a diverse range of patients (*e.g.*, skin tones). However, their broader adoption in everyday wearables is limited because they necessitate direct skin contact through electrodes, often attached to the chest. This requirement can be inconvenient for continuous, long-term monitoring. Researchers also explore IMU sensors for physiological sensing. For example, BioWatch [30] employed an IMU sensor within its design to infer physiological signals from pulse-induced vibrations. Extending this concept, [38] examined a chest-mounted IMU to gauge both HR and RR in stationary scenarios. Furthermore, [52] combined PPG and IMU sensors in a smart ring that tracks user activities and estimates HR. However, the IMU's performance can be compromised by skin contact and it may suffer from cumulative drift during long-term monitoring.

Different from the aforementioned works, MagWear delves into an alternative sensing method: biomagnetism. This approach seeks to provide inclusive and long-term physiological monitoring. Preliminary findings with MagWear have demonstrated reliable HR and RR readings across 30 subjects, accounting for variations in skin tones, body hair density, tattoos, clothing fabrics, placement, and moisture conditions.

GMR for vital sign monitoring. The realm of vital sign monitoring has witnessed a burgeoning interest in the potential of biomagnetism [17, 21, 25, 33, 34, 37, 43]. Pioneering studies [33, 37] have validated the capability of GMR sensors in detecting heartbeats when positioned on the wrist in a controlled lab environment. Furthermore, [33] has affirmed the reliability of GMR sensors for RR monitoring by benchmarking their outputs against ECG and PPG data. Concurrently, research in [21] unveiled a groundbreaking non-contact technique for Pulse Wave Velocity (PWV) estimation using GMR sensors, marking a promising avenue for future cardiovascular diagnostics. However, the theoretical capacities and practical boundaries of biomagnetism in human vital sign monitoring remain largely unexplored. Comprehensive understanding and modeling of IBF signals are conspicuously lacking. The challenge of reliably capturing IBF signals amidst human variations remains a significant hurdle.

In contrast to these earlier explorations, MagWear delves deep into the theoretical foundations of IBF signal generation, introduces an adaptive IBF tuning algorithm tailored for diverse human variations, and crafts a wristband designed for daily use. This propels the inclusive vital sign monitoring solution significantly closer to real-world adoption.

8 DISCUSSION

Comparison with alternative methods. We construct a mathematical model to serve as a theoretical foundation guiding

the design of MagWear. Different from the model-based approach, a data-driven approach could also be a potential solution. However, the data-driven approach is not our primary preference due to the limited public biomagnetism dataset. Our model-based approach reveals the fundamental issues of the biomagnetism sensing and enables us to develop an online algorithm to improve the reliability of MagWear. In addition, compared with the PPG-based method, no matter whether the traditional PPG sensor or the latest PPG sensor uses an LED-generated vector beam, our method is more inclusive and supports contactless detection. On the other hand, wireless [39–41, 49, 50] and wearable sensing are complementary solutions. Wearables can achieve long-term and effective monitoring by staying close to the user, ensuring continuous data collection. Wireless sensing relies on stationary infrastructures, they are usually deployed indoors for contactless monitoring. Hence, we believe the biomagnetism-based approach adds a new and different method for the community of human vital signs monitoring.

Extending to other potential applications. MagWear explores biomagnetism to achieve the heart rate and respiration rate monitoring. Besides, other vital signs are also promising to be detected through the variation of the IBF signal. In essence, the IBF signal is affected by the concentration of charged particles, such as iron and oxygen in the blood vessels. For example, insufficient hemoglobin or ions may lead to the symptoms of anemia and the blood oxygen index can be influenced by the change of oxygen concentration. Hence, we can further explore IBF signal variation to detect anemia and blood oxygen saturation, which is also our ongoing work.

9 CONCLUSION

We present MagWear, the first vital sign monitoring system that practically exploits biomagnetism. We implement MagWear on COTS low-cost analog components and conduct extensive experiments to evaluate its performance. Compared with the commercial Apple Watch 8, MagWear stands out for its enhanced inclusivity and robustness across various scenarios. We believe that MagWear demonstrates its viability and effectiveness, paving the way for practical integration of biomagnetism-based vital monitoring systems.

ACKNOWLEDGMENT

We thank our anonymous shepherd and reviewers for their insightful comments. This work is supported in part by the National Science Fund of China under grant No. 62202264, No. 62394344, No. U21B2007, National Key Research and Development Program of China No. 2022YFE0112600, 2022YFE0196000, Key Research and Development Program of Zhejiang Province No. 2021C03037.

REFERENCES

- [1] All Galaxy Watches. <https://www.samsung.com/levant/watches/all-watches/>.
- [2] American National Standards Institute (ANSI) specified error criterion for cardiac monitors and HR meters. <https://studylib.net/doc/18662295/ansi-aami-ec13-2002--cardiac-monitors--heart-rate-meters-...>
- [3] Apple Watch Series 8. <https://www.apple.com/apple-watch-series-8/>.
- [4] Electromagnetic induction. <https://www.techtarget.com/whatis/definition/electromagnetic-induction>.
- [5] Electromagnetic leakage of microwave oven. <https://www.bag.admin.ch/dam/bag/en/dokumente/str/nis/faktenblaetter-emf/faktenblatt-mikrowellenofen.pdf.download.pdf/faktenblatt%20mikrowellenofen%20e.pdf>.
- [6] FDA-approved device, LEPU PO6 fingertip pulse oximeter. <https://www.medicalexpo.com/prod/viatom-lepu/product-100940-1010078.html>.
- [7] Garmin Sport Watches. <https://www.garmin.com/en-US/c/wearables-smartwatches/>.
- [8] GMR sensor AA004. <https://www.digikey.cn/zh/products/detail/nve-corp-sensor-products/AA004-02E/1624606>.
- [9] Hall effect. https://en.wikipedia.org/wiki/Hall_effect.
- [10] High-current operational amplifier OPA549. <https://www.ti.com.cn/product/cn/OPA549>.
- [11] Instrumentation amplifier INA126. <https://www.ti.com/lit/ds/symlink/ina126.pdf>.
- [12] Magnet safety: continuous exposure limits guidelines. <https://blink.ucsd.edu/safety/radiation/magnet/limits.html>.
- [13] Neodymium magnets and pacemaker safety. <https://www.kjmagnetics.com/blog.asp?p=pacemaker-safety>.
- [14] Ultra-low power MCU ESP32. <https://www.espressif.com/en/products/soc/soc32>.
- [15] Ultralow offset voltage operational amplifier OP07. <https://www.analog.com/media/en/technical-documentation/data-sheets/OP07.pdf>.
- [16] Wheatstone bridge. <https://www.geeksforgeeks.org/wheatstone-bridge/>.
- [17] J. R. Bai and V. J. Kumar. Optimal design to ensure maximum coupling between magnetic flux and arterial blood in a magneto plethysmogram sensor head. *IEEE Sensors Journal*, 21(2):1417–1423, 2021.
- [18] B. Bent, B. A. Goldstein, W. A. Kibbe, and J. P. Dunn. Investigating sources of inaccuracy in wearable optical heart rate sensors. *NPJ digital medicine*, 3(1):18, 2020.
- [19] A. Byanjankar, Y. Liu, Y. Shu, I. Shin, M. Choi, and H. Kim. S-ubitap: Leveraging acoustic dispersion for ubiquitous and scalable touch interface on solid surfaces. *IEEE Transactions on Mobile Computing*, 22(11):6800–6816, 2023.
- [20] D. Castaneda, A. Esparza, M. Ghamari, C. Soltanpur, and H. Nazeran. A review on wearable photoplethysmography sensors and their potential future applications in health care. *International journal of biosensors & bioelectronics*, 4(4):195, 2018.
- [21] A. Chandrasekhar, J. Joseph, and M. Sivaprakasam. A novel magnetic plethysmograph for non-invasive evaluation of arterial compliance. In *Proceedings of IEEE EMBC*, 2016.
- [22] D. Chen, M. Wang, C. He, Q. Luo, Y. Iravantchi, A. Sample, K. G. Shin, and X. Wang. Magx: Wearable, untethered hands tracking with passive magnets. In *Proceedings of the 27th Annual International Conference on Mobile Computing and Networking*, pages 269–282, 2021.
- [23] T. Chen, X. Fan, Y. Yang, and L. Shangguan. Towards remote auscultation with commodity earphones. In *Proceedings of the 20th ACM Conference on Embedded Networked Sensor Systems*, pages 853–854, 2022.
- [24] T. Chen, L. Shangguan, Z. Li, and K. Jamieson. The design and implementation of a steganographic communication system over in-band acoustical channels. *ACM Transactions on Sensor Networks*, 2023.
- [25] V. K. Chugh, K. Kalyan, and C. S. Anoop. Feasibility study of a giant magneto-resistance based respiration rate monitor. In *Proceedings of IEEE EMBC*, 2016.
- [26] D. Cohen, E. A. Edelsack, and J. E. Zimmerman. Magnetocardiograms taken inside a shielded room with a superconducting point-contact magnetometer. *Applied Physics Letters*, 16(7):278–280, 1970.
- [27] S. Francesco, C. Gloria, S. Susanna, P. Angelica, I. Grazia, P. Riccardo, B. Alessandro, P. Salvatore, S. Lorenzo, and D. Leonardo. Photoplethysmographic sensors, potential and limitations: Is it time for regulation? a comprehensive review. *Measurement*, 218(1):113–150, 2023.
- [28] X. Guo, Y. He, and X. Zheng. Wizig: Cross-technology energy communication over a noisy channel. *IEEE/ACM Transactions on Networking*, 28(6):2449–2460, 2020.
- [29] Y. He, X. Guo, X. Zheng, Z. Yu, J. Zhang, H. Jiang, X. Na, and J. Zhang. Cross-technology communication for the Internet of Things: A survey. *ACM Computing Surveys*, 55(5):1–29, 2022.
- [30] J. Hernandez, D. McDuff, and R. W. Picard. Biowatch: estimation of heart and breathing rates from wrist motions. In *2015 9th International Conference on Pervasive Computing Technologies for Healthcare (PervasiveHealth)*, pages 169–176. IEEE, 2015.
- [31] C. Jeong, H. Yoon, H. Kang, and H. Yeom. Effects of skin surface temperature on photoplethysmograph. *Journal of Healthcare Engineering*, 5(4):429–438, 2014.
- [32] H. Jiang, J. Zhang, X. Guo, and Y. He. Sense me on the ride: Accurate mobile sensing over a lora backscatter channel. In *Proceedings of the 19th ACM Conference on Embedded Networked Sensor Systems*, pages 125–137, 2021.
- [33] K. Kalyan, V. K. Chugh, and C. S. Anoop. Non-invasive heart rate monitoring system using giant magneto resistance sensor. In *Proceedings of IEEE EMBC*, 2016.
- [34] A. J. Lopez-Martin and A. Carlesena. Performance tradeoffs of three novel GMR contactless angle detectors. *IEEE Sensors Journal*, 9(3):191–198, 2009.
- [35] M. Mansoor Baig, H. Gholamhosseini, and M. J. Connolly. A comprehensive survey of wearable and wireless ECG monitoring systems for older adults. *Medical & Biological Engineering & Computing*, 51(1):485–495, 2013.
- [36] N. Mora, F. Cocconcelli, G. Matrella, and P. Ciampolini. Fully automated annotation of seismocardiogram for noninvasive vital sign measurements. *IEEE Transactions on Instrumentation and Measurement*, 69(4):1241–1250, 2020.
- [37] C. T. Phua, G. Lissorgues, B. C. Gooi, and B. Mercier. Statistical validation of heart rate measurement using modulated magnetic signature of blood with respect to electrocardiogram. *International Journal of Bioscience, Biochemistry and Bioinformatics*, 2(2):110–116, 2012.
- [38] C. Romano, E. Schena, D. Formica, and C. Massaroni. Comparison between chest-worn accelerometer and gyroscope performance for heart rate and respiratory rate monitoring. *Biosensors*, 12(10):834, 2022.
- [39] Y. Shu, C. Bo, G. Shen, C. Zhao, L. Li, and F. Zhao. Magicol: Indoor localization using pervasive magnetic field and opportunistic WiFi sensing. *IEEE Journal on Selected Areas in Communications*, 33(7):1443–1457, July 2015.
- [40] Y. Shu, Y. Huang, J. Zhang, P. Coué, P. Cheng, J. Chen, and K. G. Shin. Gradient-based fingerprinting for indoor localization and tracking. *IEEE Transactions on Industrial Electronics*, 63(4):2424–2433, 2016.
- [41] Y. Shu, Z. Li, B. F. Karlsson, Y. Lin, T. Moscibroda, and K. Shin. Incrementally-deployable indoor navigation with automatic trace generation. In *Proceedings of IEEE Conference on Computer Communications*, 2019.

- [42] Y. Shu, K. G. Shin, T. He, and J. Chen. Last mile navigation using smartphones. In *Proceedings of ACM International Conference on Mobile Computing and Networking*, 2015.
- [43] T. Tamori and K. Akatsu. Investigation of current measurement method of bonding wire by using GMR sensor. In *Proceedings of IEEE ICPE*, 2019.
- [44] N. ui, N. Pham, J. J. Barnitz, Z. Zou, P. Nguyen, H. Truong, T. Kim, N. Farrow, A. Nguyen, J. Xiao, R. Deterding, T. Dinh, and T. Vu. eBP: A wearable system for frequent and comfortable blood pressure monitoring from user's ear. In *Proceedings of the 25th Annual International Conference on Mobile Computing and Networking*, pages 1–17, 2019.
- [45] W. Wang, Y. He, M. Jin, Y. Sun, and X. Guo. Meta-speaker: Acoustic source projection by exploiting air nonlinearity. In *Proceedings of the 29th Annual International Conference on Mobile Computing and Networking*, pages 1–15, 2023.
- [46] W. Wang, J. Li, Y. He, X. Guo, and Y. Liu. Motorbeat: Acoustic communication for home appliances via variable pulse width modulation. *Proceedings of the ACM on Interactive, Mobile, Wearable and Ubiquitous Technologies*, 6(1):1–24, 2022.
- [47] Z. Xiao, T. Chen, Y. Liu, and Z. Li. Mobile phones know your keystrokes through the sounds from finger's tapping on the screen. In *2020 IEEE 40th International Conference on Distributed Computing Systems*, pages 965–975. IEEE, 2020.
- [48] K. Yang, X. Zheng, J. Xiong, L. Liu, and H. Ma. Wiimg: pushing the limit of wifi sensing with low transmission rates. In *2022 19th Annual IEEE International Conference on Sensing, Communication, and Networking (SECON)*, pages 1–9. IEEE, 2022.
- [49] J. Zhang, R. Xi, Y. He, Y. Sun, X. Guo, W. Wang, X. Na, Y. Liu, Z. Shi, and T. Gu. A survey of mmwave-based human sensing: Technology, platforms and applications. *IEEE Communications Surveys & Tutorials*, 2023.
- [50] J. Zhang, Y. Zhou, R. Xi, S. Li, J. Guo, and Y. He. Ambiear: Mmwave based voice recognition in NLoS scenarios. *Proceedings of the ACM on Interactive, Mobile, Wearable and Ubiquitous Technologies*, 6(3):1–25, 2022.
- [51] X. Zheng, J. Wang, L. Shangguan, Z. Zhou, and Y. Liu. Design and implementation of a csi-based ubiquitous smoking detection system. *IEEE/ACM Transactions on Networking*, 25(6):3781–3793, 2017.
- [52] H. Zhou, T. Lu, Y. Liu, S. Zhang, R. Liu, and M. Gowda. One ring to rule them all: An open source smartring platform for finger motion analytics and healthcare applications. In *Proceedings of the 8th ACM/IEEE Conference on Internet of Things Design and Implementation*, pages 27–38, 2023.